Journal article:

Carman Yueng, Ching Tai Ng. (2020). Nonlinear guided wave mixing in pipes for detection of material nonlinearity. Journal of Sound and Vibration, 485:115541

Nonlinear Guided Wave Mixing in Pipes for Detection of Material Nonlinearity

Carman Yeung and Ching Tai Ng[1]

School of Civil, Environmental & Mining Engineering, The University of Adelaide, 5005 SA, Australia

Abstract

Pipes have multiple applications in daily life and they are subjected to different types of defects. Nonlinear guided wave has attracted significant attention in detecting microstructural change at early stage of material deterioration. Extensive research using wave mixing with different wave modes has focused on plate-like structures. However, limited experimental studies have been conducted on the detection of material nonlinearity in pipes using two interacting guided waves. This study investigates nonlinear features generated due to mixing of torsional guided waves and material nonlinearity in pipes at low frequency range. The nonlinear theory of elasticity is implemented in a three-dimensional (3D) finite element (FE) method to simulate the effect of material nonlinearity on torsional guided wave mixing. The phenomenon of nonlinear features generated due to torsional guided wave mixing is investigated by 3D FE models. There is good agreement between the data obtained in the laboratory and numerical simulation results. This study demonstrates the existence of the combinational harmonic generation experimentally and provides physical insight into the phenomenon of nonlinear wave mixing. The findings of this study can further advance the damage detection techniques based on material nonlinearity in wave mixing.

[1] Corresponding author: alex.ng@adelaide.edu.au

Keywords: Guided wave, wave mixing, material nonlinearity, finite element simulation, pipe, torsional wave, circular waveguide

1. Introduction

Non-destructive evaluation (NDE) technique is important for safety-critical structures, such as pipelines. Time-dependent loads result in material degradation in metallic structures. Cracks developed in degrading materials may cause catastrophic failures if proper structural investigation has not been done to identify damage at early stage. Studies focused on using ultrasonic guided wave have been carried out in the literature [1]. Ultrasonic guided waves are one of the reliable NDE techniques. The benefits includes the high sensitivity to small defects and a relatively large inspection area [2]-[3]. Linear ultrasonic guided waves can also interrogate inaccessible location of structures and provide online condition monitoring of in-service structures [4].

Torsional guided wave has an advantage of long-range damage detection in pipelines. Fundamental axisymmetric torsional mode of guided wave T(0,1) has attracted increasing attention due to its nondispersive characteristic [5]. The use of low frequency is preferential for actuating torsional waves experimentally since less wave modes are generated at low frequency range. Carandente and Cawley [6] carried out an experimental study on the T(0,1) mode in a frequency range around 100kHz. Geometrical change due to various defects in pipes, such as corrosion [7], notch [8] and delamination [9], can be identified using linear guided wave scattered from the damage. In most of the situations, baseline measurement is essential [10]-[11] to extract the damage information which is limited to macro-scale. To address these restrictions of linear guided wave methods, research has focused on adopting nonlinear features of guided waves because this approach is highly sensitive to micro-scale damage [12].

Many studies on nonlinear guided waves have focused on contact and material nonlinearity [13]-[15]. Examples of contact nonlinearity have fatigue cracks and loosening [16]-[18]. Material nonlinearity is primarily induced by the interaction with discontinuities at lattice level, such as micro-cracks and voids. In the time-domain signals, the nonlinear features do not show significant difference compared to linear guided wave responses in terms of scattering and mode conversion. However, the distortion due to the nonlinear elastic wave behaviours of a material has a significant change after the transformation to frequency-domain [19]. By studying material nonlinearity, nonlinear guided wave provides damage information at higher order harmonics in frequency-domain. They are always the integral multiples of the incident wave frequency. In most of the cases, higher harmonic generation [20] caused by the contact and/or material nonlinearity can be applied to baseline-free damage detection because baseline data from pristine condition of the structure is not necessary for this approach. Liu *et al.* [21] conducted a study on shear horizontal wave for the generation of Rayleigh-Lamb secondary mode in plates. Ideally, primary Rayleigh-Lamb mode should not appear if shear horizontal wave is generated. However, due to finite width transducers, they concluded that non-planar wavefront leads to the generation of both primary and secondary harmonics in Rayleigh-Lamb wave.

Research focused on harmonic generation in cylindrical waveguide has been conducted theoretically and experimentally [22]-[24] using single frequency guided wave. Liu *et al.* [14] carried out analytical studies for the second harmonics generation from different modes which were applicable to simple pipe-like structures. Chillara and Lissenden [25] used longitudinal mode of guided wave to study the nonlinear features in pipes. Li and Cho [26] measured second harmonics with thermal fatigue damage in pipes. Choi *et al.* [27] applied the fundamental torsional mode of guided wave in pipe-like structures and measured the higher harmonic generation. Li *et al.* [28] investigated the generation of second harmonics due to material

nonlinearity in tube-like structures. However, it is potentially difficult to distinguish the cause of nonlinearity between weakly material nonlinearity and instrumentation nonlinearity. The nonlinear distortion can be induced by measurement systems, such as amplifiers and transducers [29].

Due to the generation of undesired higher harmonic from equipment, relevant research work has been focused on the feasibility of combinational harmonic generation induced by the mix of two incident waves at different frequencies [30]-[31]. It has been demonstrated that guided wave mixing is sensitive to material degradation [32]. The harmonics are generated at sum and difference of the excitation frequencies due to guided wave mixing for damage detection. Early development of the guided wave mixing focused on bulk waves [33]. It can be used to detect contact acoustic nonlinearity (CAN) induced by imperfect bond interfaces in structures [34]. Alston *et al.* [35] investigated CAN in aluminium specimens using two incident waves propagating in different directions. The wave mixing technique can also be applied to different materials. Demčenko *et al.* [36] implemented bulk wave mixing method to study different dynamic processes in polymers, such as ageing problem. McGovern *et al.* [37] used the mixing of two bulk waves in non-collinear direction to study the nonlinear response in concrete structures. However, the use of bulk wave is ineffective as the inspection area is very limited, which is much smaller than Rayleigh wave and Lamb wave.

Research on wave mixing has been gradually extended to Lamb waves [38]-[39] because they are capable of selecting multiple wave modes for damage detection and able to provide large inspection area. Jingpin *et al.* [29] mixed two Lamb waves with different excitation frequencies in plates using collinear interaction approach. They investigated the generation of combinational harmonics due to the Lamb wave mixing phenomenon. Hassanian and Lissenden [32] studied the generation of secondary combinational harmonics at sum and difference of excitation frequencies in plate-like structures due to wave mixing. They

demonstrated that material defects appeared in plates can be characterised by studying material nonlinearity. Extensive studies have been done on bulk wave mixing and Lamb wave mixing to study the phenomenon of combinational harmonic generation. However, a very limited experimental investigation has been carried out on combinational harmonic generation due to torsional wave mixing in pipes. The purpose of this study is to carry out experimental validation for the existence of the combinational harmonics generated by torsional guided wave mixing in pipe-like structures and the measured results are also compared with three-dimensional (3D) finite element (FE) simulations.

The paper is organised as follows. Section 2 introduces the guided wave mixing approach and the theory of elasticity for material nonlinearity. The 3D scanning laser vibrometer is used to collect experimental data in Section 3. Section 4 applies the weakly nonlinear elasticity in FE method. The development of the FE model can confirm the experiment conducted in this study, and provide the framework for more complex studies in future. In Section 5, the 3D FE model of a pipe is described and validated using experimentally measured data. This section also studies the sensitivity of the combinational harmonic generation due to torsional wave mixing in relation to different levels of fatigue damage. Finally, conclusions are drawn in Section 6.

2. Nonlinear guided wave mixing techniques

2.1 Generation of combinational harmonics

The generation of combinational harmonics requires the interaction of two or more wave sources. Using two wave sources as an example, mixed frequency (f_1 & f_2) is composed by two incident waves at frequencies f_1 and f_2, where $f_2 > f_1$. It not only induces their corresponding second order harmonics (i.e. $2f_1$ and $2f_2$), but also generates the combinational harmonics at

their sum and difference frequencies when mixing the waves. Figure 1a shows a schematic frequency spectrum which indicates the interaction of fundamental waves and the combinational second harmonic generation due to wave mixing. For more practical application, a single excitation point of two individual wave sources has the advantage to provide convenient access because it only requires one-side access to implement the ultrasonic guided wave mixing. The wave mixing zone indicated in Figure 1b represents the interaction of the wave mixing.

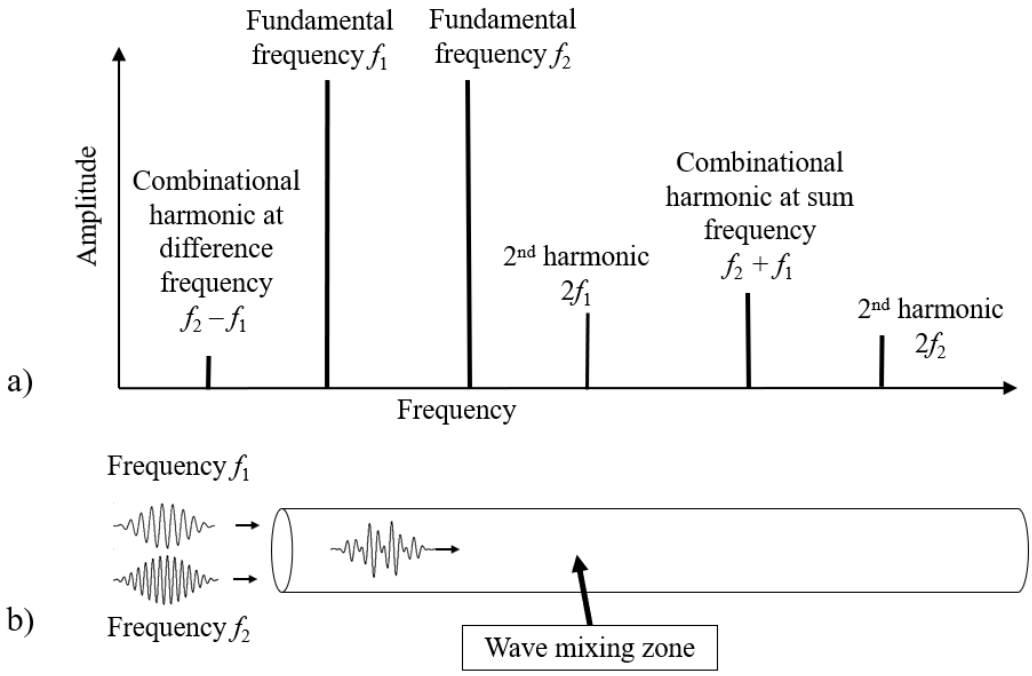

[Figure 1 Schematic diagram of a) frequency spectrum for ultrasonic guided wave mixing, and b) wave mixing zone in pipe]

2.2 Theoretical framework for weakly nonlinear elasticity

The following FE modelling framework for material nonlinearity not only can be used in simple structures, but also can apply to complicated configurations. In order to gain physical insights of combinational harmonic generation for wave mixing in pipes, this study aims to

have experimental validation by a FE model with the aid of nonlinear strain energy function. The derivation of nonlinear guided wave equation is based on continuum mechanics. The interaction of wave propagation is regarded as an infinitesimal deformation. The deformation gradient **F** (Figure 2) can quantify the change of a shape and the rigid rotation of a material. [13]

$$\mathbf{ds} = \mathbf{F}\mathbf{dS} = \frac{\partial \mathbf{s}}{\partial \mathbf{S}} d\mathbf{S} \tag{1}$$

where **S** is the position of the material particle in the stress-free reference configuration located at **s** in the current configuration.

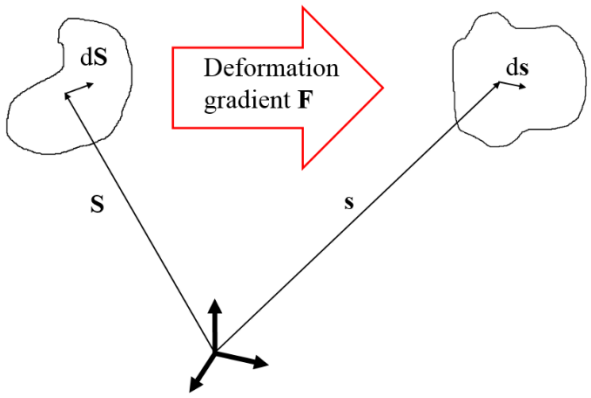

[Figure 2. Illustration of deformation gradient]

The right Cauchy-Green strain tensor **C** considers the rigid body translation between configurations. This strain tensor is symmetric and can be related to **F** as below

$$\mathbf{C} = \mathbf{U}^2 = \mathbf{F}^{\mathrm{T}}\mathbf{F} \tag{2}$$

where **U** is the right stretch tensor for local stretching at **S**. It is noted that **C** and **U** are the material tensors. The Green-Lagrange strain tensor **E** is used in the nonlinear strain energy function.

$$\mathbf{E} = \frac{1}{2}(\mathbf{F}^{\mathrm{T}}\mathbf{F} - \mathbf{I}) \tag{3}$$

where **I** is the identity tensor. It is noted that **E** is also symmetric. Polar decomposition is a way to separate the deformation gradient into the rotation tensor and the stretch tensor.

$$\mathbf{F} = \mathbf{RU} \tag{4}$$

R is an orthogonal tensor for local rotation of the material at **S**.

$$\mathbf{R}^{-1} = \mathbf{R}^{\mathrm{T}} \tag{5}$$

where det **R**=1

The governing equation used in the theory of elasticity (Eq, (6)) refers to the strain energy function *W*, where the strain is in the second order terms. To perform a small amplitude wave motion in an elastic object, the function *W* is presented in the Green-Lagrange strain tensor **E**. This particular form of strain tensor allows the expansion of the strain energy function to the third order. The equations are capable of studying nonlinear guided waves since they take material nonlinearity into consideration due to the inclusion of the third order terms. Based on the study of Murnaghan [41] , the expansion of the nonlinear strain energy function *W* can be written as

$$W(\mathbf{E}) = \frac{1}{2}(\lambda + 2\mu)i_1^2 + \frac{1}{3}(l + m)i_1^2 - 2\mu i_2 - 2mi_1 i_2 + ni_3 \tag{6}$$

where λ and μ are the Lamé elastic constants; *l*, *m* and *n* are the third order elastic constants. The principal invariants of **E** (i_1, i_2 and i_3) are given by

$$i_1 = tr\mathbf{E}$$

$$i_2 = \frac{1}{2}[i_1^2 - tr(\mathbf{E})^2]$$

$$i_3 = det\mathbf{E} \tag{7}$$

The second Piola-Kirchhoff (PK2) stress is obtained by the partial derivation of $W(\mathbf{E})$ with respect to $\mathbf{E}$, i.e. $\frac{\partial W(E)}{\partial E}$. The Cauchy stress can be written in terms of the PK2 stress and the deformation gradient as below

$$\boldsymbol{\sigma} = \mathrm{J}^{-1}\mathbf{F}\frac{\partial \mathrm{W}(\mathbf{E})}{\partial \mathbf{E}}\mathbf{F}^{\mathrm{T}} \tag{8}$$

where $\mathrm{J}^{-1}$is the Jacobian determinant and equals to $\det(\mathbf{F})$.

3. Excitation using piezoceramic transducers and measurements using 3D scanning laser Doppler vibrometer

This section illustrates the mixing of torsional waves at two different excitation frequencies and the details of the excitation using piezoceramic transducers and measurements using 3D scanning laser Doppler vibrometer [43] to investigate the material nonlinearity of torsional wave mixing phenomenon in an aluminium pipe. Figure 3 is a schematic diagram of the experimental setup used in this study. The outer diameter of the pipe is r = 25mm with wall thickness of 1.5mm. The excitation of torsional guided wave was achieved by four square-shaped piezoceramic shear transducers (Ferroperm Pz27) with dimensions of 6mm×6mm×1mm. Reflective spray was coated on the surface of the pipe specimen to improve the signal-to-noise ratio of the signals measured by the 3D scanning laser vibrometer.

Two excitation signals with low frequencies at f_1 = 70 kHz and f_2 = 110 kHz were used in the laboratory test to avoid less complication of multi-modes. The combined frequency excitation signal was achieved by merging the two single frequency excitation signals together. The signal at frequency f_1 lagged behind the signal at frequency f_2 for 22μs in the pre-mixing procedure. Hann-windowed tone burst pulses [42] of 6 and 13 cycles at f_1 and f_2 were employed, respectively. The actual excitation from the actuators in time-domain was measured by the

laser Doppler vibrometer and is shown in Figure 4a. The Fast Fourier Transform (FFT) was employed to transform the time-domain data to the frequency-domain data for analysis. Figure 4b shows the corresponding response in frequency-domain. The excitation signal was generated by a computer-controlled signal generator. The peak-to-peak output voltage was amplified by a power amplifier to 120V.

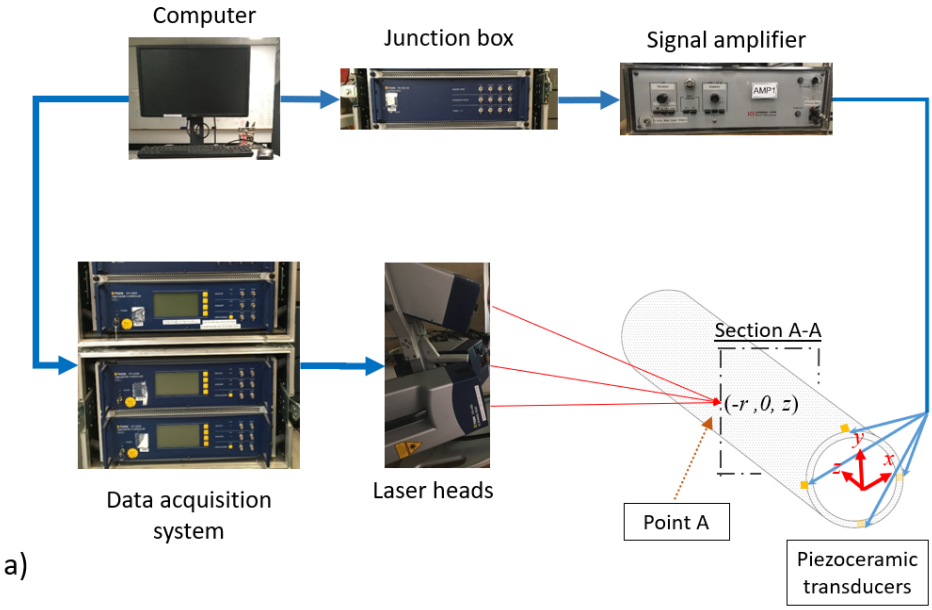

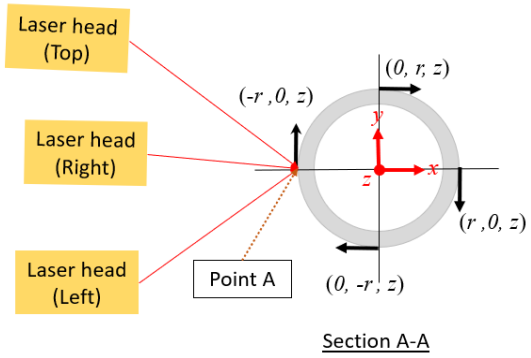

[Figure 3. a) Experimental setup of piezoceramic shear transducers, 3D laser Doppler vibrometer and the pipe specimen, b) cross-section of the pipe specimen]

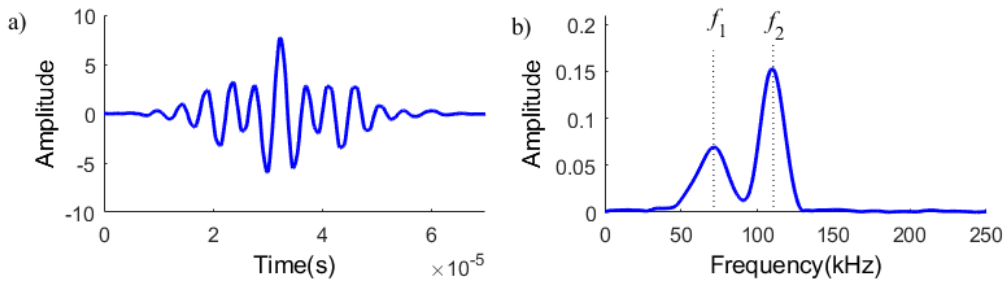

[Figure 4. Actual mixed frequency excitation from actuators measured by laser Doppler vibrometer, a) time-domain and b) frequency-domain]

The experimental data was collected using Polytec high-frequency 3D scanning laser Doppler vibrometer (PSV-400-3D-M). Low-pass filter with the cut-off frequency of 600kHz and signal averaging with 2000 acquisitions were applied to enhance the signal-to-noise ratio of the measured data. This 3D laser scanning system is for non-contact optical vibration measurement. It consists of three spatially independent laser scanning heads. Figure 3b indicates the measurement locations in Cartesian coordinate system (i.e. in-plane horizontal x, in-plane vertical y and out-of-plane z). The measurements were done by using the three heads at the measurement point. The intersection point of the laser beams measures the velocity fields. Section A-A in the same figure illustrates that the velocities in tangential and longitudinal directions were measured simultaneously at Point A. The torsional wave has the maximum signal magnitude in tangential direction.

Figures 5a and 5b present the time-domain experimentally measured mixed frequency waves in torsional (tangential) and longitudinal direction, respectively. Figures 5c and 5d show the corresponding signals in frequency-domain. The measurement point is at 450mm away from the excitation location. The time-domain signals are normalised by the maximum signal amplitude so that the harmonics are comparable for the subsequent sections.

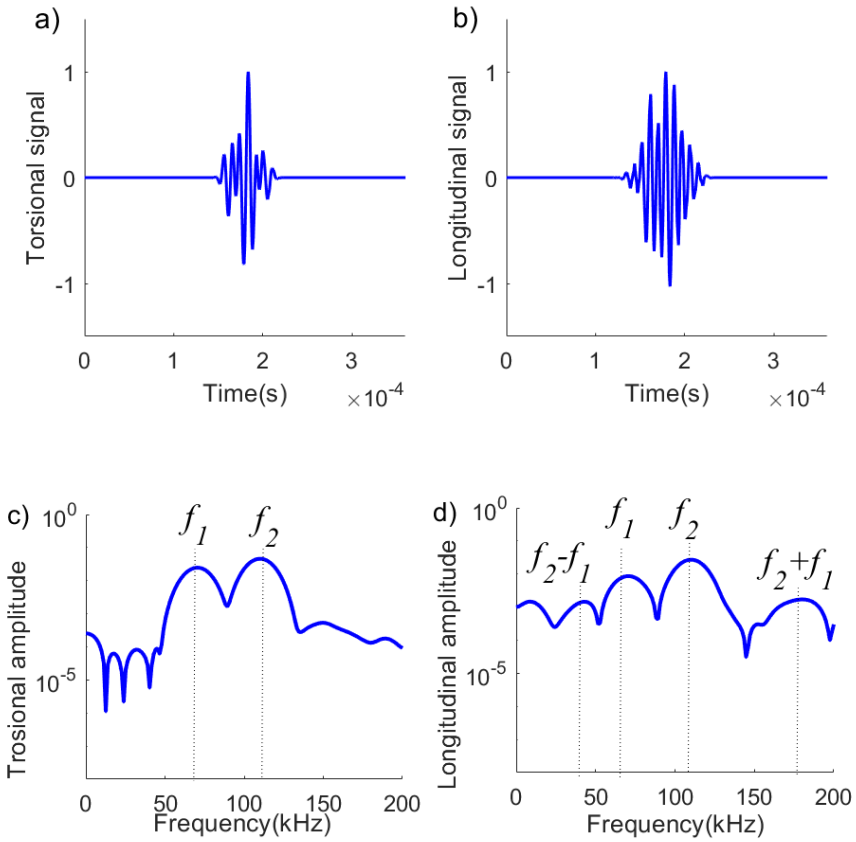

[Figure 5. Experimentally measured of time-domain signal in a) torsional direction and b) longitudinal direction, and c)-d) corresponding signals in frequency-domain]

Figure 6 compares the experimentally obtained single and mixed frequency responses in frequency-domain. In this experimental study, the generation of combinational harmonics are the main focus which are highlighted in Figure 6b. Three different tests were carried out in the study. The first test used the fundamental frequency f_1 excitation signal. The second test used the fundamental frequency f_2 excitation signal. The third test used the mixed frequencies (f_1 & f_2) excitation signal. They are indicated using black dotted line, red solid line and blue solid line in Figure 6, respectively. The tangential motion of the fundamental torsional guided wave mode shall not give second harmonics in wave mixing. Previous study [14] used analytical method and stated this point of view at single frequency. However, very limited research was carried out to experimentally confirm the generation of combination harmonics

in torsional wave mixing for material nonlinearity. Therefore, the current study focuses on the combinational harmonics generation due to guided wave mixing and experimentally validates this phenomenon.

It is expected that no higher harmonics appear in the torsional direction when the two incident waves interact with each other in Figure 6. Apart from the fundamental frequency at f_1 and f_2, the combinational harmonics at difference frequency ($f_2 - f_1$ = 40 kHz) and sum frequency ($f_2 + f_1$ = 180 kHz) have obvious peaks in the longitudinal measurement, which are highlighted by dotted vertical lines.

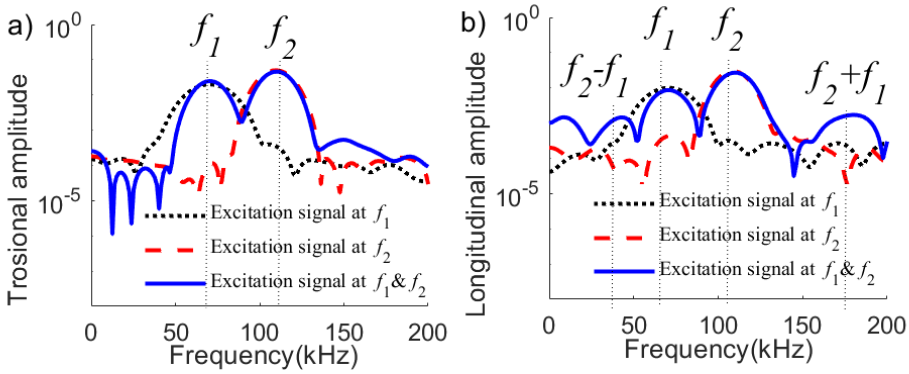

[Figure 6. Experimentally measured single and mixed frequency velocity responses in frequency-domain, a) torsional and b) longitudinal directions]

4. Three-dimensional finite element model of pipes

In this study, a 3D FE model was used to simulate guided wave mixing for the phenomenon of material nonlinearity. The excitation location was the same excitation position in the pipe specimen using in the experiment. The geometry of the pipe model was created and meshed in ABAQUS. The pipe is modelled by eight-node linear brick elements with hourglass control and reduced integration (C3D8R). The in-plane dimension of the element is approximately 0.25mm×0.25mm to ensure the simulation is stable. This ensures that there are at least 20 and 25 FE nodes per wavelength for torsional wave and longitudinal wave. The thickness of the

elements is 0.25mm so there are six layers of elements in the thickness direction (Figure 7a). The dynamic simulation is solved by ABAQUS/Explicit. The density and Young's modulus of the aluminium are 2700 kg/m^3 and 69GPa, respectively. The Lame's and third order elastic constants used in the user-defined subroutine are listed in Table 1.

[Table 1. Lame's and third order elastic constants of aluminium used in the FE simulations (in GPa)]

Lame's constants		Third order elastic constants		
λ	μ	l	m	n
54.9	26.5	-252.2	-325	-351.2

A layout of the pipe modelled using FE method is shown in Figure 7. As shown in Figure 7a, the incident T(0,1) waves at f_1 and f_2 excitation frequencies were excited by applying tangential point loads at four edges of the circumference located at the pipe end. The coordinate of Point B is (r,0,0), which has the measured velocity in v_y. This is the maximum signal magnitude of the torsional wave in y direction. The longitudinal wave signal can be obtained from the nodal displacement in z direction. The study used the same frequencies and number of cycles Hann-windowed tone burst pulses used in experiment as the excitation signals. This study considered three different situations in the excitation signals at low frequency range, which are fundamental frequency f_1 excitation signal, fundamental frequency f_2, excitation signal, and pre-mixed frequencies (f_1 & f_2) excitation signal. The three situations considered in FE are the same as in the experimental study. The existence of combinational harmonics at the sum and difference frequencies can be associated with the induction of shear coupling from the fundamental torsional waves to longitudinal waves at the combinational harmonic frequencies. Thus, the data in the FE simulations were extracted in both the torsional and longitudinal directions. Figures 8a and 8b show the numerically simulated time-domain signals in tangential and longitudinal directions at the location of 500mm from the excitation location. The corresponding data in frequency domain are shown in Figures 8c and 8d. The FE model

includes the nonlinear strain function (Section 2.2) to simulate the effect of material nonlinearity.

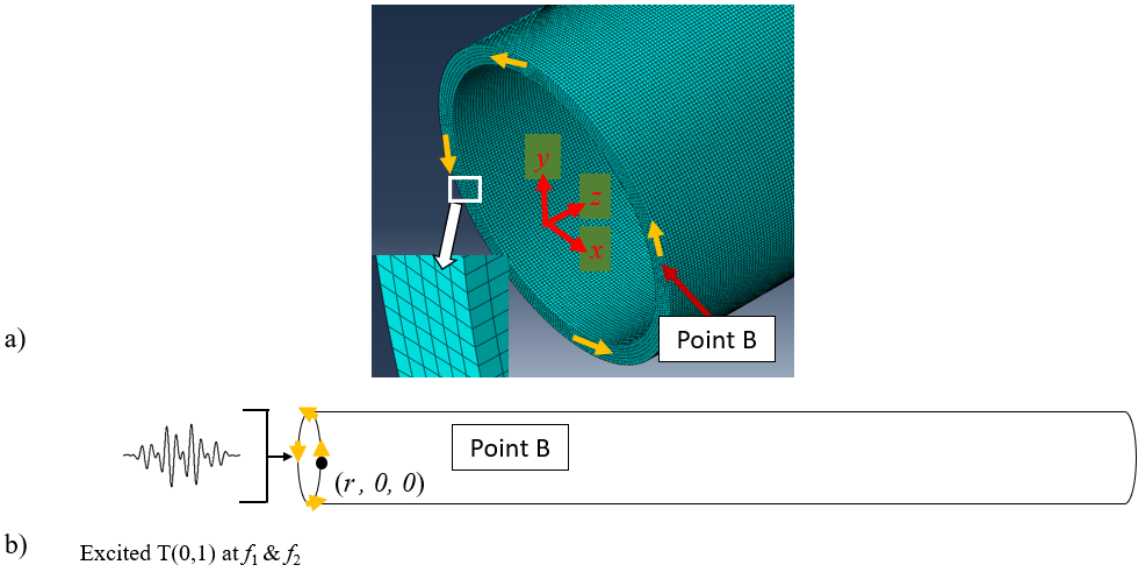

[Figure 7 a) 3D FE model and T(0,1) mode excitation b) schematic diagram of the configuration used in the FE model]

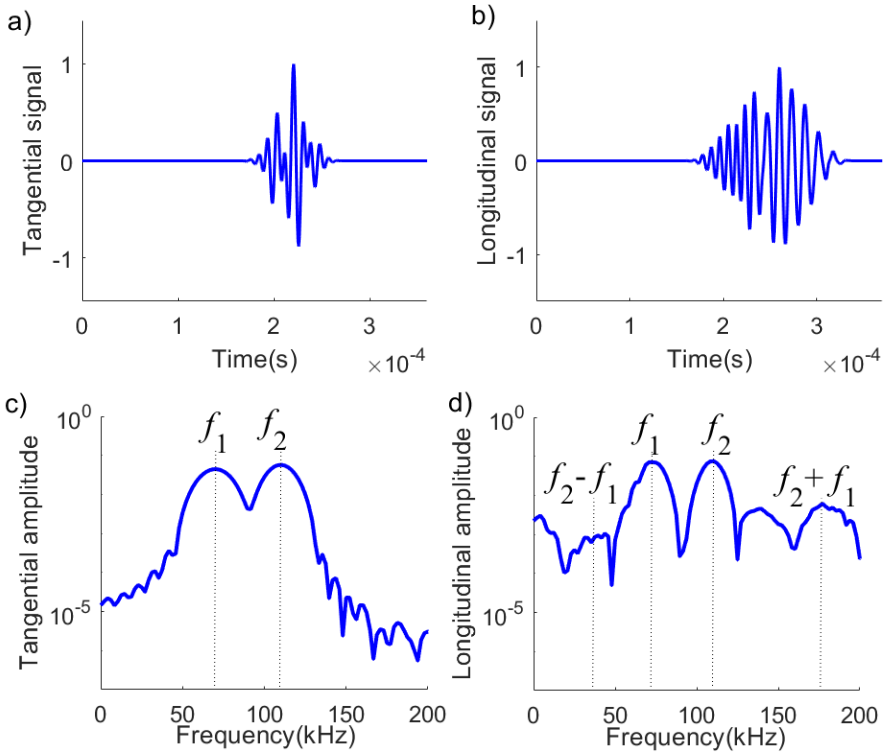

[Figure 8 Numerical simulated time-domain signals in a) tangential direction and b) longitudinal direction, and c)-d) the corresponding signals in frequency-domain]

Figure 9 shows the phase velocity dispersion curves for the torsional and longitudinal wave modes from 50 kHz to 330 kHz in steps of 20 kHz. The signals at five measurement points were recorded and used to calculate the averaged phase velocity at each excitation frequency. The first measurement is located at 300mm from the excitation signal and the distance between two consecutive measuring points is 1mm. Therefore, the separation of two measurement points is less than one half of the incident wave wavelength. The following equation is used to calculate the phase velocity

$$c_p = \frac{2\pi f \Delta y}{\Delta \varphi} \tag{9}$$

where f is the central frequency of the incident wave, Δy is the distance between the two measurements and $\Delta \varphi$ is the change in phase angle.

Results calculated by a software DISPERSE [44] is used to compare with the results calculated from FE simulation data in Figure 9. The theoretical calculation is indicated by dashed lines while the FE data is indicated by square markers. The T(0,1) mode and L(0,1) mode are represented by blue and red colours, respectively. The FE calculations are in agreement with the theoretical values. Thus, the FE model can accurately predict both the torsional and longitudinal wave propagations.

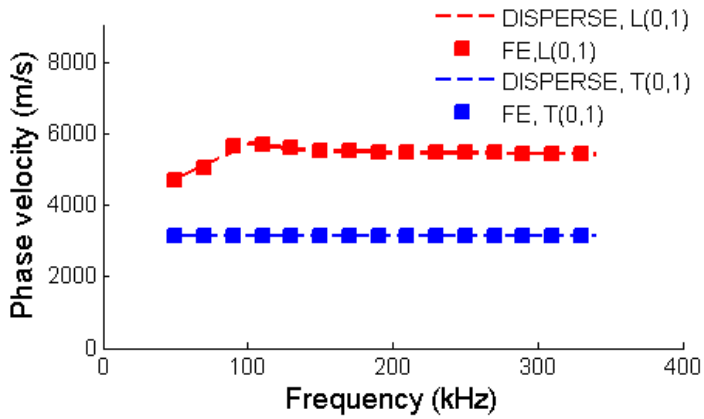

[Figure 9. Phase velocity dispersion obtained from DISPERSE and FE simulation]

5. Experimental validation 3D FE model with nonlinear elasticity

Figure 10 is the comparison between the data from the FE model with the consideration of material nonlinearity and the experimentally measured mixed frequency response. FFT was used for the conversion in experimental and numerical data. The results from the experiment and the FE model were normalised to allow direct comparison. The blue solid line and the red dotted line refer to the FE simulated frequency spectra and the experimentally measured frequency spectra, respectively. The corresponding frequencies are labelled in Figure 10. The FFT signals simulated by the nonlinear FE model in the tangential and longitudinal directions generally share the same pattern with those signals in the experiment. It implies that the direction of torsional force for the nonlinear FE model does not generate any combinational harmonics.

The generation of primary and combinational harmonics at sum and difference frequencies (i.e. $f_2 \pm f_1$) can be observed in the longitudinal motion (Figure 10b). It should be noted that the primary harmonics at f_1 and f_2 in the longitudinal direction are induced because of the non-planar wavefront generated by finite width transducers [21]. In the current study, the excitations in the experiments and simulations were four individual piezoceramic transducers at the end of the pipe. This produces non-planar wavefront, and hence, it induces the primary harmonics at f_1 and f_2 in the longitudinal direction. Therefore, the longitudinal signal contains both primary and combinational harmonic frequencies when mixed frequency torsional wave is generated."

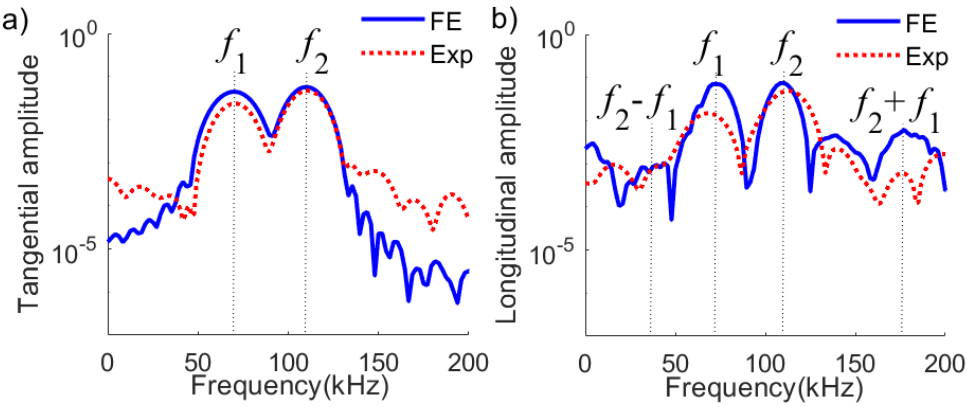

[Figure 10. Mixed frequency response of FE simulation and experimentally measured data in a) tangential and b) longitudinal directions]

5.1. Simulation results and discussion

In this section, two FE models were used to simulate the guided wave responses. The FE model with the use of the material subroutine VUMAT [45] which implemented extended Murnaghan's strain energy equation in Section 2.2 is labelled as nonlinear FE (blue solid line) in the figure. The other model is a benchmark simulation which does not take into account the material nonlinearity. The corresponding FFT response is labelled as linear FE (black dashed line) in the figure. Figures 11 and 12 show the measured data in both directions for individual excitation frequencies f_1 and f_2. The linear and nonlinear signals do not have much difference in the tangential direction (Figures 11a and 12a).

Since the primary fundamental torsional waves cannot generate second harmonic torsional waves, the second harmonic does not appear in those plots. Only the peaks at the excitation frequencies, which are the fundamental frequency components, appear in the tangential direction. Instead, there are additional peaks at $2f_1$ and $2f_2$ in nonlinear FE. It is demonstrated that the modified strain energy function with third order terms in Eq. (6) can effectively model the nonlinear guided wave behaviours through the utilisation of user

subroutine. The second harmonics at $2f_1$ and $2f_2$ appear in the data measured in longitudinal direction (Figures 11b and 12b). In the meantime, no harmonic appears in the linear response (black dashed lines) at the double frequency of the excitation signals.

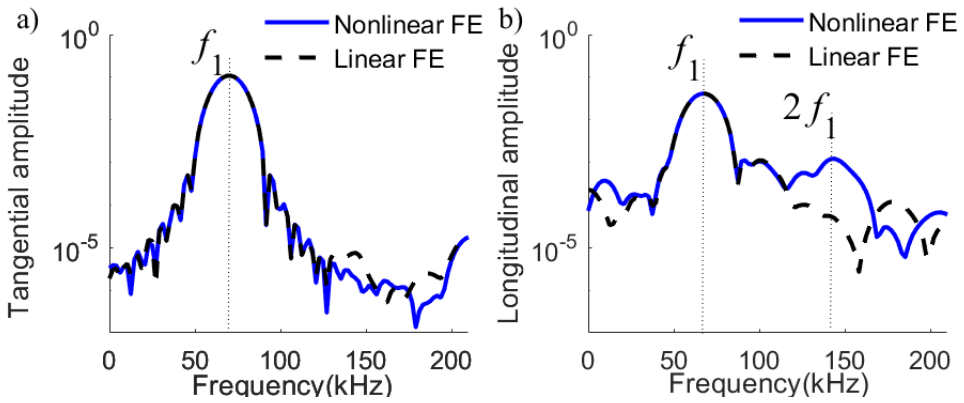

[Figure 11. FE model verification of single frequency at f_1 in a) tangential and b) longitudinal directions]

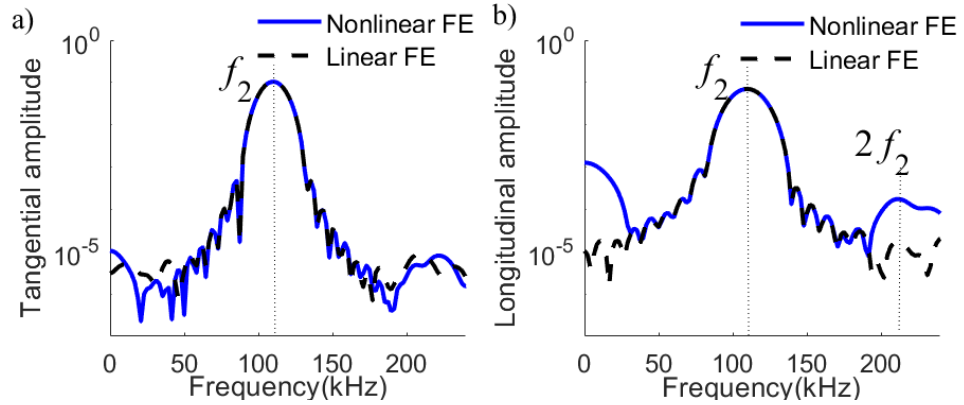

[Figure 12. FE model verification of single frequency at f_2 in a) tangential and b) longitudinal directions]

Similarly, Figure 13a shows that the signal does not contain any second harmonic components in the data calculated in the tangential direction. In Figure 13b, the combinational harmonic at the sum frequency ($f_2 + f_1$) is approximately 20% higher than at the difference

frequency ($f_2 - f_1$). Due to the mutual wave interaction [25], the combinational harmonics at the sum and difference frequencies can be observed in the mixed frequency response. It is noticeable that single frequency excitation does not generate the combination harmonics at sum and different frequencies since they are originally from the mutual interaction of two waves. Therefore, none of these combinational harmonic components can be observed in the measured data using single frequency excitation at f_1 and f_2, respectively.

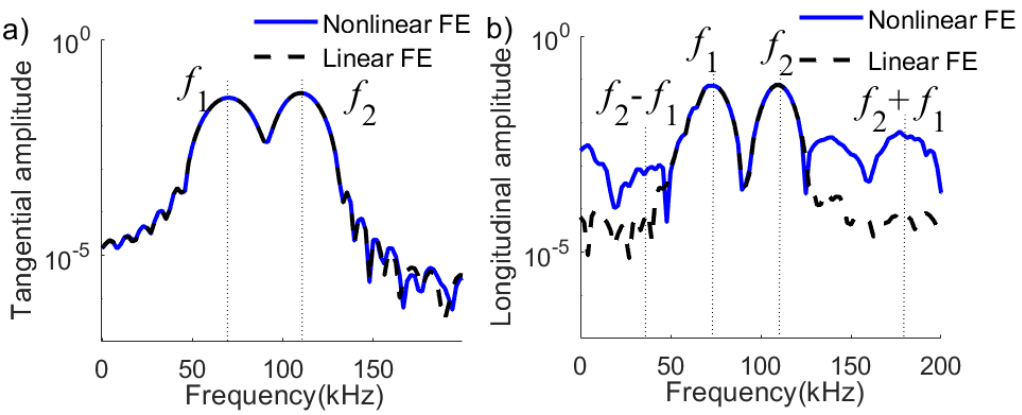

[Figure 13. Mixed frequency response in frequency domain for FE models in a) tangential and b) longitudinal directions]

5.2. Effect on relative nonlinear parameter in material nonlinearity at different fatigue stages

This section presents a study to relate the relative nonlinear parameter with the several stages of evenly distributed fatigue damage growth using FE simulations. A material with various fatigue states subjected to the accumulation of dislocation substructures leads to the change in the value of higher harmonics. This can be applied to the combinational harmonics in nonlinear guided wave mixing in pipes to characterise the fatigue damage of a material quantitatively. The relative nonlinear parameter β' is defined as [40]

$$\beta' = \frac{A_3}{A_1 A_2} \tag{10}$$

where A_3 is the amplitude of the harmonic wave and A_1, A_2 are the amplitudes of the two incident waves. The parameter β' can used as an indicator as the term A_3 is the generation of combinational harmonic frequencies in the incident wave frequency signal. It can monitor the material nonlinearity quantitatively prior to the initiation of micro-cracks. An accurate experimental study about the fatigue damage of aluminium was carried out in the previous research [46] which provided convincible data at different stages in an evenly distributed fatigue damage cycle. The relevant data is shown in Table 2.

[Table 2. Material properties of aluminium at three different stages in a fatigue life cycle (in GPa)[46]]

Third order elastic constants \ Fatigue life (%)	0	40	80
l	-149.4	-153.7	-155.9
m	-102.8	-113.2	-115.3
n	-351.2	-358.3	-359.8

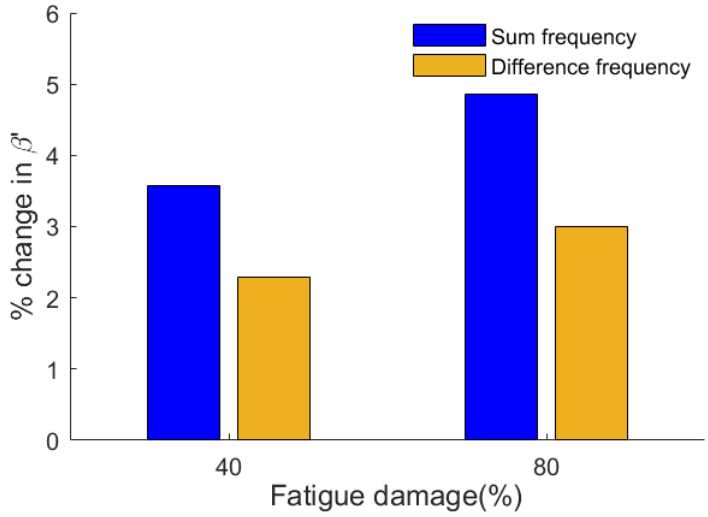

[Figure 14. Percentage change in the nonlinear parameter calculated from the FE simulation against the fatigue damage]

In order to allow direct comparison between the sum and difference harmonics, the data is expressed in percentage change for the relative nonlinear parameter β' when the fatigue life

is at 40% and 80%. As shown in Figure 14, the combinational harmonics at sum and difference frequencies are indicated by blue colour and yellow colour, respectively. The measurement points are at the distance of 450mm away from the excitation points. The increase in β' at sum frequency is more obvious than that at difference frequency. The overall value of β' at difference frequency is about a half of the value of β' at sum frequency.

6. Conclusions

The study of guided wave mixing of two fundamental torsional waves in pipe-like structures has been investigated numerically and experimentally. The 3D scanning laser Doppler vibrometer was used in the experiment. The generation of combinational harmonics due to guided wave mixing in pipes has been measured in experiment. They were induced at the sum and difference frequencies of the incident waves in longitudinal direction when the two T(0,1) mode waves interact with each other. The modified Murnaghan's energy equation to third order terms was implemented in the 3D FE model to capture the combinational harmonic generation in guided wave mixing. There are good agreement between the frequency responses of experimental measurements and numerical simulations. The experimentally validated 3D FE model has been used to investigate the generation of combinational harmonics with increasing percentage of fatigue damage level. Current investigations are focusing on extending the study to higher order harmonic generation due to material nonlinearity using guided wave mixing.

Acknowledgement

This work was funded by the Australian Research Council (ARC) under the grant number DP200102300. The authors are grateful to this support.

Appendix

In this study, the material nonlinearity is taken into account in the 3D FE model. A set of equations are implemented through a user subroutine VUMAT in ABAQUS/Explicit to analyse the effect of material nonlinearity on guided wave mixing in pipes. The stress in ABAQUS is the Cauchy stress tensor $\boldsymbol{\sigma}$ in the basis of Green-Naghdi rate.

$$\widehat{\boldsymbol{\sigma}} = \mathbf{R}^{\mathrm{T}}\boldsymbol{\sigma}\mathbf{R} \tag{A.1}$$

Using Eq. (4), (6), (8) and (A.1), the stress in ABAQUS can be interpreted as

$$\begin{aligned}\widehat{\boldsymbol{\sigma}} &= \mathrm{J}^{-1}\mathbf{R}^{\mathrm{T}}\mathbf{F}\frac{\partial W(\mathbf{E})}{\partial \mathbf{E}}\mathbf{F}^{\mathrm{T}}\mathbf{R} \\ &= \mathrm{J}^{-1}\mathbf{R}^{\mathrm{T}}\mathbf{R}\mathbf{U}\frac{\partial W(\mathbf{E})}{\partial \mathbf{E}}\mathbf{U}^{\mathrm{T}}\mathbf{R}^{\mathrm{T}}\mathbf{R} \\ &= \mathrm{J}^{-1}\mathbf{U}\frac{\partial W(\mathbf{E})}{\partial \mathbf{E}}\mathbf{U}^{\mathrm{T}}\end{aligned} \tag{A.2}$$

The values of $\mathbf{U}$ and $\mathbf{F}$ at the end of final time step (t) will be updated in the stress equations at the end of an integration step $(t + \Delta t)$ and renewed in stressNew(i).

References

[1] N. Chakraborty, V.T. Rathod, D.R. Mahapatra, S. Gopalakrishnan, Guided wave based detection of damage in honeycomb core sandwich structures, *NDT & E Int.* **49** (2012) 27-33

[2] G.T. Pudipeddi, C.T. Ng, A. Kotousov, Mode conversion and scattering of Lamb waves at delaminations in composite laminate, *J Aerospace Eng ASCE* **32** (2019) 04019067.

[3] S. Mariani, T. Nguyen, R. R. Phillips, P. Kijanka, F. Lanza di Scalea, W.J. Staszewski , G. Carr, Noncontact ultrasonic guided wave inspection of rails, *Struct. Health Monit.* **12** (2013) 539-548

[4] J.M. Hughes, J. Vidler, C.T. Ng, A. Khanna, M. Mohabuth, L.F. Rose, A. Kotousov, Comparative evaluation of in situ stress monitoring with Rayleigh waves, *Struct. Health Monit.* **18** (2019) 205-215

[5] H. Kwun, S.Y. Kim, M.S. Choi, S.M. Walker, Torsional guided-wave attenuation in coal-tar-enamel-coated, buried piping, *NDT & E Int.* **37** (2004) 663-665

[6] R. Carandente, P. Cawley, The effect of complex defect profiles on the reflection of the fundamental torsional mode in pipes, *NDT & E Int.* **46** (2012) 41-47

[7] P.B. Nagy, F. Simonetti, G. Instanes, Corrosion and erosion monitoring in plates and pipes using constant group velocity Lamb wave inspection, *Ultrasonics* **54** (2014) 1832-1841

[8] C. Yeung, C.T. Ng, Time-domain spectral finite element method for analysis of torsional guided waves scattering and mode conversion by cracks in pipes, *Mech. Syst. Signal Process.* **128** (2019) 305-317

[9] J. Bingham, M. Hinders, Lamb wave detection of delaminations in large diameter pipe coatings, *Open Acoust. J.* **2** (2009) 75-86

[10] K.Y. Jhang, Nonlinear ultrasonic techniques for nondestructive assessment of micro damage in material: a review, *Int. J. Precis. Eng. Man.* **10** (2009) 123-135

[11] J.L. Rose, A baseline and vision of ultrasonic guided wave inspection potential, *J. Pressure Vessel Technol.* **124** (2002) 273-282

[12] Y. Shen, C.E.S. Cesnik, Modeling of nonlinear interactions between guided waves and fatigue cracks using local interaction simulation approach, *Ultrasonics* **74** (2017) 106-123

[13] Y. Yang, Ng, C.T. Ng, M. Mohabuth, A. Kotousov. Finite element prediction of acoustoelastic effect associated with Lamb wave propagation in pre-stressed plates, *Smart Mater Struct* **28** (2019) 095007

[14] Y. Liu, E. Khajeh, C.J. Lissenden, J.L. Rose, Interaction of torsional and longitudinal guided waves in weakly nonlinear circular cylinders, *J. Acoust Soc. Am.* **133** (2013) 2541-2553

[15] H. Sohn, H.J. Lim, M.P. DeSimio, K. Brown, M. Derriso, Nonlinear ultrasonic wave modulation for online fatigue crack detection, *J. Sound Vib.* **333** (2014) 1473-1484

[16] Y. Yang, C.T. Ng, A. Kotousov, Bolted joint integrity monitoring with second harmonic generated by guided waves, *Struct. Health Monit.* **18** (2019) 193-204

[17] C. Pruell, J.Y. Kim, J. Qu, L.J. Jacobs Evaluation of fatigue damage using nonlinear guided waves, *Smart Mat. Struct.* **18** (2009) 035003

[18] Y. Yang, C.T. Ng, A. Kotousov, Influence of crack opening and incident wave angle on second harmonic generation of Lamb waves, *Smart Mater Struct* **27** (2018) 055013

[19] A. Pau, F. Lanza di Scalea, Nonlinear guided wave propagation in prestressed plates, *J. Acoust. Soc. Am.* **137** (2015) 1529-1540

[20] C.T. Ng, H. Mohseni, H.F. Lam, Debonding detection in CFRP-retrofitted reinforced concrete structures using nonlinear Rayleigh wave, *Mech. Syst. Sig. Process*. **125** (2019) 245-256

[21] Liu, Y., Chillara, V. K., & Lissenden, C. J. (2013). On selection of primary modes for generation of strong internally resonant second harmonics in plate. *Journal of sound and vibration*, *332*(19), 4517-4528.

[22] Z. Liu, Q. Xu, Y. Gong, C. He, B. Wu, A new multichannel time reversal focusing method for circumferential Lamb waves and its applications for defect detection in thick-walled pipe with large-diameter, *Ultrasonics* **54** (2014) 1967-1976

[23] Y. Wang, J.D. Achenbach, The effect of cubic material nonlinearity on the propagation of torsional wave modes in a pipe, *J. Acoust Soc. Am.* **140** (2016) 3874-3883

[24] X. Guo, D. Zhang, J. Zhang, Detection of fatigue-induced micro-cracks in a pipe by using time-reversed nonlinear guided waves: A three-dimensional model study, *Ultrasonics* **52** (2012) 912-919

[25] V.K. Chillara, C.J. Lissenden, Analysis of second harmonic guided waves in pipes using a large-radius asymptotic approximation for axis-symmetric longitudinal modes, *Ultrasonics* **53** (2013) 862-869

[26] W. Li, Y. Cho, Thermal fatigue damage assessment in an isotropic pipe using nonlinear ultrasonic guided waves, *Exp. Mech.* **54** (2014) 1309-1318

[27] G. Choi, Y. Liu, C.J. Lissenden, Nonlinear guided waves for monitoring microstructural changes in metal structures, *ASME 2015 Pressure Vessels and Piping Conference* (2015)

[28] W. Li, M. Deng, Y. Cho, Cumulative second harmonic generation of ultrasonic guided waves propagation in tube-like structure, *J. Comput. Acoust.* **24** (2016) 1650011

[29] J. Jingpin, M. Xiangji, H. Cunfu, B. Wu, Nonlinear Lamb wave-mixing technique for micro-crack detection in plates, *NDT & E Int.* **85** (2017) 63-71

[30] Y. Ishii, S. Biwa, T. Adachi, Non-collinear interaction of guided elastic waves in an isotropic plate, *J. Sound Vib.* **419** (2018) 390-404

[31] N. Li, J. Sun, J. Jiao, Wu B, C. He, Quantitative evaluation of micro-cracks using nonlinear ultrasonic modulation method, *NDT & E Int.* **79** (2016) 63-72

[32] M. Hasanian, C.J. Lissenden, Second order ultrasonic guided wave mutual interactions in plate: Arbitrary angles, internal resonance, and finite interaction region, *J. Appl. Phys.* **124** (2018) 164904

[33] Z. Chen, G. Tang, Y. Zhao, L.J. Jacobs, J. Qu, Mixing of collinear plane wave pulses in elastic solids with quadratic nonlinearity, *J. Acoust. Soc. Am.* **136** (2014) 2389-2404

[34] J. Jiao, H. Lv, C. He, B. Wu, Fatigue crack evaluation using the non-collinear wave mixing technique, *Smart Mat. Struct.* **26** (2017) 065005

[35] J. Alston, A. Croxford, J. Potter, P. Blanloeuil, Nonlinear non-collinear ultrasonic detection and characterisation of kissing bonds, *NDT & E Int.* **99** (2018) 105-116

[36] A. Demčenko, V. Koissin, V.A. Korneev, Noncollinear wave mixing for measurement of dynamic processes in polymers: Physical ageing in thermoplastics and epoxy cure, *Ultrasonics* **54** (2014) 684-693

[37] M.E. McGovern, W.G. Buttlar, H. Reis, Characterisation of oxidative ageing in asphalt concrete using a non-collinear ultrasonic wave mixing approach, *Insight: Non-Destructive Testing and Condition Monitoring* **56** (2014) 367-374

[38] F. Li, Y. Zhao, P. Cao, N. Hu, Mixing of ultrasonic Lamb waves in thin plates with quadratic nonlinearity, *Ultrasonics* **87** (2018) 33-43

[39] A.K. Metya, S. Tarafder, K. Balasubramaniam, Nonlinear Lamb wave mixing for assessing localized deformation during creep, *NDT & E Int.* **98** (2018) 89-94

[40] A.J. Croxford, P.D. Wilcox, B.W. Drinkwater, P.B. Nagy, The use of non-collinear mixing for nonlinear ultrasonic detection of plasticity and fatigue, *J. Acoust. Soc. Am.* **126** (2009) EL117-EL122

[41] F.D. Murnaghan, Finite deformations of an elastic solid, *Am. J. Math.* **59** (1937) 235-260

[42] S. He, C.T. Ng, Modelling and analysis of nonlinear guided waves interaction at a breathing crack using time-domain spectral finite element method. *Smart Mater. Struct.* **26** (2017) 085002.

[43] W.J. Staszewski, B.C. Lee, R. Traynor, Fatigue crack detection in metallic structures with Lamb waves and 3D laser vibrometry, *Meas. Sci. Technol.* **18** (2007) 727

[44] B. Pavlakovic, M.J.S.Lowe, DISPERSE: A System for Generating Dispersion Curves, User's Manual Version 2.0.16B, *Imperial College, University of London, London* (2003)

[45] Y. Yang, C.T. Ng, A. Kotousov. Second-order harmonic generation of Lamb wave in prestressed plates, *J Sound Vib*. **460** (2019) 114903.

[46] X. Wan, P.W. Tse, G.H. Xu, T.F. Tao, Q. Zhang, Analytical and numerical studies of approximate phase velocity matching based nonlinear S0 mode Lamb waves for the detection of evenly distributed microstructural changes, *Smart Mat. Struct.* **25** (2016) 045023